

Molecular Mechanics of Silk Nanostructures Under Varied Mechanical Loading

Graham Bratzel,^{1,2} Markus J. Buehler¹

¹ Laboratory for Atomistic and Molecular Mechanics, Department of Civil and Environmental Engineering, Massachusetts Institute of Technology, Cambridge, MA, USA

² Department of Mechanical Engineering, Massachusetts Institute of Technology, Cambridge, MA, USA

Received 19 August 2011; accepted 29 September 2011

Published online 24 October 2011 in Wiley Online Library (wileyonlinelibrary.com). DOI 10.1002/bip.21729

ABSTRACT:

Spider dragline silk is a self-assembling tunable protein composite fiber that rivals many engineering fibers in tensile strength, extensibility, and toughness, making it one of the most versatile biocompatible materials and most inviting for synthetic mimicry. While experimental studies have shown that the peptide sequence and molecular structure of silk have a direct influence on the stiffness, toughness, and failure strength of silk, few molecular-level analyses of the nanostructure of silk assemblies, in particular, under variations of genetic sequences have been reported. In this study, atomistic-level structures of wildtype as well as modified MaSp1 protein from the *Nephila clavipes* spider dragline silk sequences, obtained using an *in silico* approach based on replica exchange molecular dynamics and explicit water molecular dynamics, are subjected to simulated nanomechanical testing using different force-control loading conditions including stretch, pull-out, and peel. The authors have explored the effects of the poly-alanine length of the *N. clavipes* MaSp1 peptide sequence and identify differences in nanomechanical loading conditions on the behavior of a unit cell of 15 strands with 840–990 total residues used to represent a cross-linking β -sheet crystal node in the network within a fibril of the dragline silk thread. The specific loading condition used,

representing concepts derived from the protein network connectivity at larger scales, have a significant effect on the mechanical behavior. Our analysis incorporates stretching, pull-out, and peel testing to connect biochemical features to mechanical behavior. The method used in this study could find broad applications in *de novo* design of silk-like tunable materials for an array of applications. © 2011 Wiley Periodicals, Inc. *Biopolymers* 97: 408–417, 2012.

Keywords: biological material; molecular structure; genetic sequence; critical length scale; size effect; nanostructure; molecular modeling; materiomics; spider silk

This article was originally published online as an accepted preprint. The “Published Online” date corresponds to the preprint version. You can request a copy of the preprint by emailing the *Biopolymers* editorial office at biopolymers@wiley.com

INTRODUCTION

Spider silk is an extraordinary biomaterial that surpasses most synthetic fibers in terms of toughness through a balance of ultimate strength and extensibility.^{1–5} The source of spider silk’s remarkable properties has been attributed to the specific secondary and tertiary structures of proteins found in the repeating units of spider silk,⁶ which self-assemble into a hierarchical fibrillar structure. Experimental studies have primarily focused on mapping the repeating sequence units of spider silk and the basic structural building blocks and crystallinity of fibrils. The webs of higher spiders, including the Golden

Correspondence to: M. J. Buehler; e-mail: mbuehler@MIT.EDU

© 2011 Wiley Periodicals, Inc.

Orb-Weaver *Nephila clavipes*, are composed of different kinds of silk, each with distinct mechanical properties that are adapted for the purpose of the respective part of the web. Major ampullate silk, the strongest kind of silk, is used for the dragline as well as the spokes and outer frame.⁷ Two distinct proteins are typically found in dragline silks with similar sequences across species.⁸ The dragline silk of *N. clavipes*, one of the most-studied spider silks, contains major ampullate spidroin MaSp1 and MaSp2 proteins with different repeat units and distinct mechanical functions.^{6,9–11} MaSp1 contains poly-alanine (A)_n and (GA) domains within glycine-rich (GGX)_n repeats, where X typically stands for alanine (A), tyrosine (Y), leucine (L), or glutamine (Q). Studies have suggested that MaSp1 is more prevalent in the spider dragline silk than MaSp2, with a ratio of approximately 3:2 or higher, depending on the species.^{9,12–14}

Recent investigations have revealed that antiparallel β -sheet crystals play a key role in defining the mechanical properties of silk by providing stiff cross-linking domains embedded in a semi-amorphous, Gly-rich network with extensible hidden-length.^{15–19} Studies have also shown that the hydration level and solvent conditions (e.g., ion content and pH) play a large role in the structure and mechanical properties of silk proteins^{20,21} and even the transition from concentrated dope to final silk in the spinning duct. Variations in crystallinity and alignment within the silk thread, for example, due to the reeling speed of the collected sample, have also been mapped to macroscopic mechanical properties by affecting the formation of the β -sheet crystals.^{22,23} These cross-linking β -sheet crystals use a dense network of aligned hydrogen bonds^{18,19}, have dimensions of a few nanometers, and constitute at least 10–15% of the silk volume.

The existence of 3_{10} -helices and β -turn or β -spiral conformations has been suggested for the amorphous domains.^{15–17,24} It is anticipated that novel statistical mechanics approaches,²⁵ experimental methods, such as X-ray diffraction and scattering,^{26,27} solid-state nuclear magnetic resonance^{3,11,28,29} and Raman spectroscopy,^{17,30,31} combined with multiscale atomistic-modeling methods such as those based on density functional theory^{18,32} or molecular dynamics^{18,33–35} will provide further insight into the atomic resolution structure for spider silk and similarly complex materials. An earlier study of dragline silk using replica exchange molecular dynamics (REMD)¹⁸ has yielded the first atomistic results in comparison with experimental structure identification methods.^{11,16,36} Building on this work, a systematic analysis of sequence–structure correlations using REMD and atomistic-level structural models with explicit solvent equilibration has recently been reported.³⁷ However, this study represents only a small fraction of the many

spidroin proteins of diverse species and genii. The availability of powerful new methods to computationally design and experimentally synthesize varied protein materials from the bottom up and with full control over the amino acid sequence will open exciting opportunities to engineer materials beyond spider silk for specific mechanical properties and other functional purposes.

MATERIALS AND METHODS

Spider silk filaments are composed of cross-linked extended proteins with distinct typical repeating sequence units: the poly-Ala (A)_n repeat unit and the Gly-rich (GGX)_n repeat unit, where X is another prescribed amino acid. Experimental studies of recombinant silk^{21,38} suggest that mechanical shear within a narrowing elongational flow extends and aligns MaSp oligomers during spinning into a cross-linked semi-amorphous filament network (Figure 1a). Mimicking this process, the test case structures (Figure 1b) used in this study represent a β -sheet crystal and surrounding semi-amorphous network. Previous computational studies have shown that the extended and aligned poly-Ala units in the MaSp1 sequence amyloidize into β -sheet nanocrystals, with important implications for the mechanical properties that emerge as a result of the nanocomposite.^{18,37,39} The extended partial polypeptide chains used in this study are composed of a single poly-Ala repeat with one instance of the Gly-rich semi-amorphous repeat unit on each side. Thus, the wildtype *N. clavipes* MaSp1 partial peptide sequence used in this study, in one-letter amino acid code, is: (GGAGQGGYGGGLGSQGAGRGLGGQGAG)(AAAAAA)(GGAGQGGYGGGLGSQGAGRGLGGQGAG), with repeat units marked by parentheses. The wildtype poly-Ala length of six residues is systematically varied to the artificial lengths of 2-Ala and 12-Ala to study the effect of this unit's length, and thus β -sheet crystal size, on mechanical behavior. Test structures total between 840 and 990 residues, depending on the poly-Ala length.

Nanomechanical Testing

Nanomechanical testing is performed on each equilibrated test case of poly-Ala length with TIP3P explicit solvent. Each test is simulated at 300 K using the NAMD molecular modeling program and CHARMM-22 force field with explicit water solvent. To prevent the protein from interacting with its image across the periodic boundary after large deformation of the protein, the simulation box with fully wrapping periodic boundary conditions, is kept larger than the expected deformed size, and pressure control is disabled. While some water molecules become gaseous during this type of simulation, it is verified that most of the water maintains a liquid state surrounding the protein. Particle Mesh Ewald⁴⁰ electrostatics is used to better capture solvent effects and solvent-mediated changes in secondary structure.

Three types of force-controlled tests are performed: stretch, pull-out, and peel. Since the names of the mechanical tests are common, the authors capitalize them in this study to emphasize the specific loading conditions used in this study in contrast to other mechanical tests of silk proteins. These types of tests are based on the possible loading conditions of a single β -sheet crystal within the fibrillar network may experience, in which, strands of a given crystal diverge to separate crystals further in the network, as illustrated

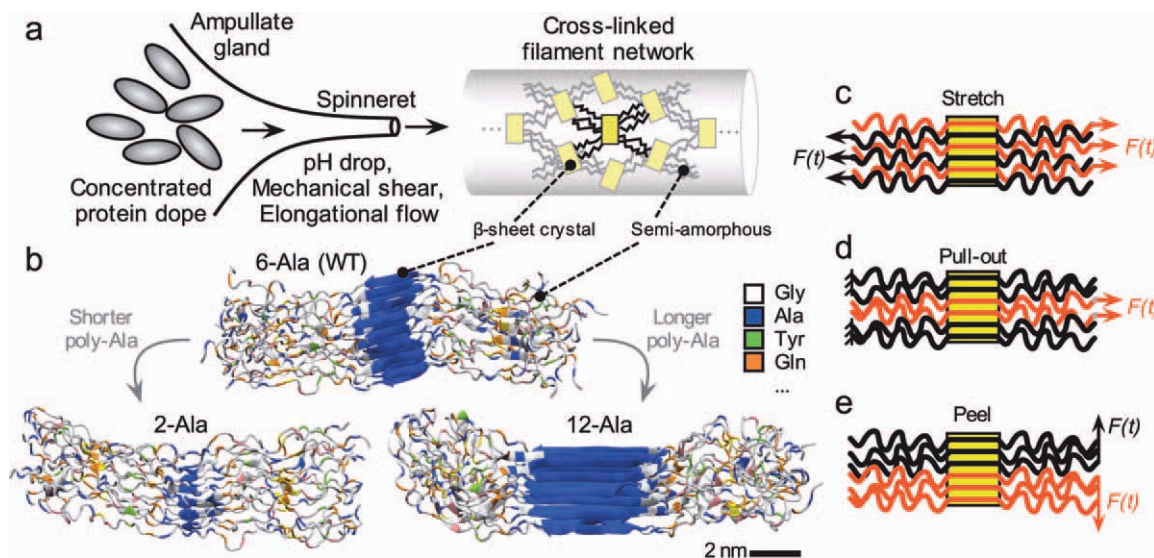


FIGURE 1 Mimicry of natural elongational flow and test loading conditions. (a) A combination of chemistry and shear flow transform the concentrated protein dope into a filament network cross-linked by β -sheet crystals; based on insight gained from experimental work.²¹ (b) Predicted β -sheet crystals and surrounding semi-amorphous strands for cases of 2-Ala, 6-Ala (wildtype), and 12-Ala. Colored by amino acid; explicit water is hidden for clarity. (c) The stretch test loads alternative strands, while (d) the pull-out test loads two central strands within a constrained unit cell. (e) The peel test splits the unit cell perpendicular to the β -sheet direction.

in Figure 1a. The Stretch test loading conditions are based on a uniformly loaded network, as in earlier work on the wildtype sequence using implicit solvent.⁴¹ The pull-out test is hypothesized to better represent the nonuniform loading of diverging strands, in which, only a few strands of a given crystal are loaded before the others. During the stretch and pull-out tests, the force $F(t)$ on each loaded alpha-carbon terminus is increased by a step of 20 pN every 20 ps of equilibration. While previous studies of a similar MaSp1 unit cell with an implicit solvent model used steps of 2 pN every 20 ps,⁴¹ using explicit solvent in the present study with a sufficient simulation box size results in a tenfold increase in particle count and necessitates the increase in loading rate. The specific loading conditions of each type of test are described in more detail below.

Stretch Test. The stretch test loads the β -sheet crystal in multi-lap shear and is based on previous computational studies of the wildtype 6-Ala case.⁴¹ Figure 1c shows a schematic of the stretch test loading conditions: 14 strands are loaded by their terminal alpha-carbon in opposing directions for multi-lap shear. This leads to Mode II slipping failure of multiple interfaces along the strands, especially H-bonds along the β -sheets but also including H-bonds within the semi-amorphous regions. To maintain a null net force, an even number of strands are loaded, and the remaining 15th strand is left free. The simulation is complete when the protein has failed in shear, i.e., when one or more strands have separated from the main body.

Pull-out Test. The pull-out test loads the β -sheet crystal in double shear and is chosen to better represent the probable loading conditions of a fringed micelle poly-crystalline material, in which, strands within a crystal diverge and connect to separate crystals further in

the fibrillar network. Figure 1d shows a schematic of the pull-out test loading conditions. The terminal alpha-carbons of 13 strands are fixed, while the termini of the remaining two central strands are loaded. This is similar to simple shear but prevents a bending moment and subsequent tilting of the interface out of pure Mode II loading. The simulation is complete when the protein has failed in shear, i.e., when one or more loaded strands have separated from the main body.

Peel Test. The peel test cleaves the β -sheet crystal in the H-bond direction and is chosen to supplement the pull-out loading conditions of a fringed micelle poly-crystalline material, in which, strands within a crystal diverge and connect to separate crystals further in the fibrillar network. Figure 1e shows a schematic of the peel test loading conditions. The terminal alpha-carbons of 14 strands are separated into two equal groups that minimize strand entanglement and cleave the crystal cleanly. These groups are then loaded in opposite transverse directions. To maintain a null net force, an even number of strands are loaded, and the remaining 15th strand is left free. The force $F(t)$ on each loaded alpha-carbon terminus is increased by a step of 10 pN every 40 ps of equilibration. Two peeling cases are considered: starting from the lamellar equilibrated structure and another starting with the “crack” tip at the edge of the β -sheet crystal. Testing is complete when the two halves of the unit cell have separated. During testing, the unloaded end of the protein does not displace.

Secondary Structure Analysis

The instantaneous secondary structure content of each equilibrated structure is determined using the STRIDE algorithm built into the

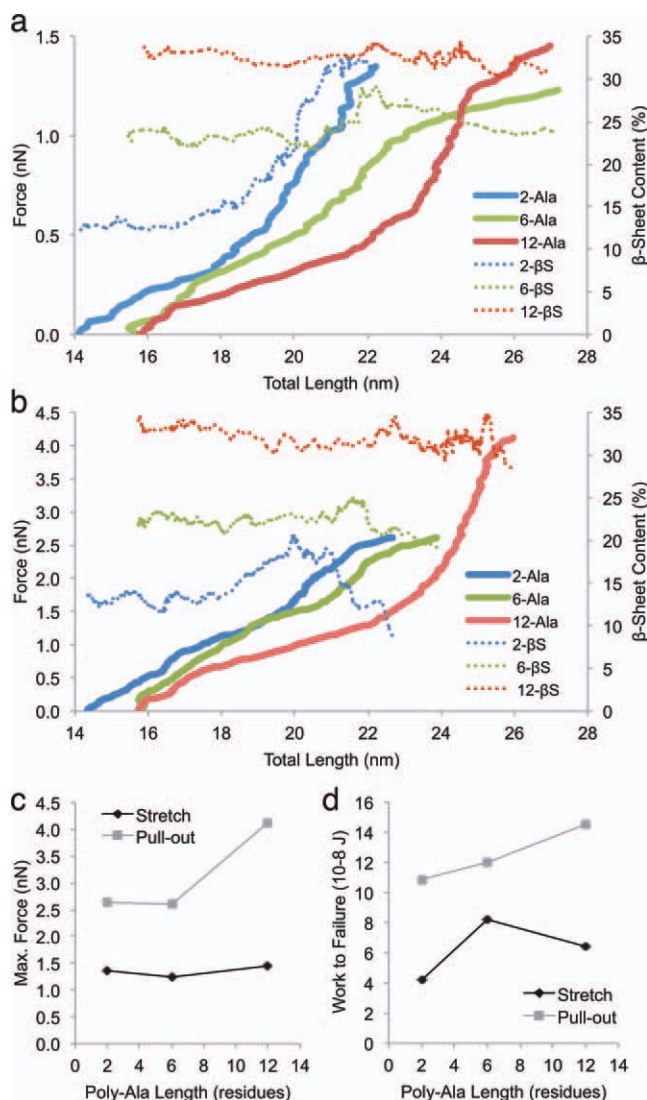


FIGURE 2 Nanomechanical analysis results for (a) stretch and (b) pull-out testing. Force is shown in a solid line, while β -sheet content is dotted. (c) The force at failure and (d) the work to failure depend on poly-Ala length as well as the loading conditions, suggesting an adaptation of the crystal to in situ pull-out conditions.

VMD Molecular Graphics Viewer⁴² and customized.tcl scripts. The STRIDE algorithm holds an advantage over DSSP and other secondary structural algorithms using pattern recognition of statistically derived backbone dihedral angle information.⁴³

RESULTS AND DISCUSSION

The failure forces of the stretch tests show negligible dependence on the poly-Ala length, which correlates directly with the crystal length in the backbone direction. In particular, failure forces are found to be 1.35 nN for the 2-Ala case; 1.23 nN for the 6-Ala case; and 1.45 nN for the 12-Ala case (Figure 2a). The deformation profiles are similar for each test case and

show a common strain-hardening around 0.5 nN. A final softening regime is observed between the strain-hardening regime and failure. This is especially evident in the 6-Ala case and is attributed to a solvent-mediated molecular analog of ductility that prevents catastrophic failure in favor of deformation. This also greatly increases the work-to-failure, i.e., the area under the force–deformation curve. Although the 6-Ala case fails at a slightly lower force than the 2-Ala case, it extends approximately 5 nm longer before failure and thus requires a much larger work-to-failure, as seen in Figure 2d. Despite beginning between 12 and 33% β -sheet depending on poly-Ala length, as seen in Figures 2a and 2b, the average β -sheet content of each test case shows a peak near 20–35% preceding failure due to a strain-induced elongation and parallel alignment of random coil conformations and subsequent localized transition to β -sheet,⁴⁴ thereby changing the final effective crystal length (in the backbone direction) despite the initial conditions. Further analysis of the correlation between β -sheet content and stiffness is discussed in later sections.

The failure forces of the pullout tests are approximately twice as large as those of the stretch test (1.9–2.4 times greater) and are also greater for the 12-Ala cases than for the 2-Ala or 6-Ala case. In particular, failure forces are found to be 2.62 nN for the 2-Ala case; 2.60 nN for the 6-Ala case; and 4.12 nN for the 12-Ala case, a 60% increase over the other poly-Ala cases (Figure 2c). The deformation profiles (Figure 2b) are similar in shape to those during the stretch test and show a similar strain-hardening, though later in this study at 1.50 nN. A third, softened regime is observed between the strain-hardened regime and failure, similar to – but shorter than – the third regime seen in stretch tests with explicit solvent. The delayed yielding and superior strength of the 12-Ala cases are attributed to the fundamental differences in the pull-out test loading conditions when compared with those of the stretch test. In the stretch test, each strand is nearly uniformly extended, and the structure becomes brittle. In the pull-out tests, only two central strands are loaded, and the load is able to be transferred over adjacent strands that can be more readily deformed and extended. This load transfer and deformation leads to a pseudo-plastic zone that surrounds the loaded central strands and allows greater ductility than in stretch tests. For the 12-Ala case, the crystal provides a larger pseudo-plastic zone, visualized in Figure 4, and more work-to-failure is required to transfer the load through the crystal to adjacent, non-loaded strands (Figure 2d). Changes in the total β -sheet content during deformation are less severe than for the stretch tests, changing by only 5–7% over the entire simulation. This is a direct result of only the crystal and pseudo-plastic regions being sufficiently deformed to trigger β -sheet transitions.

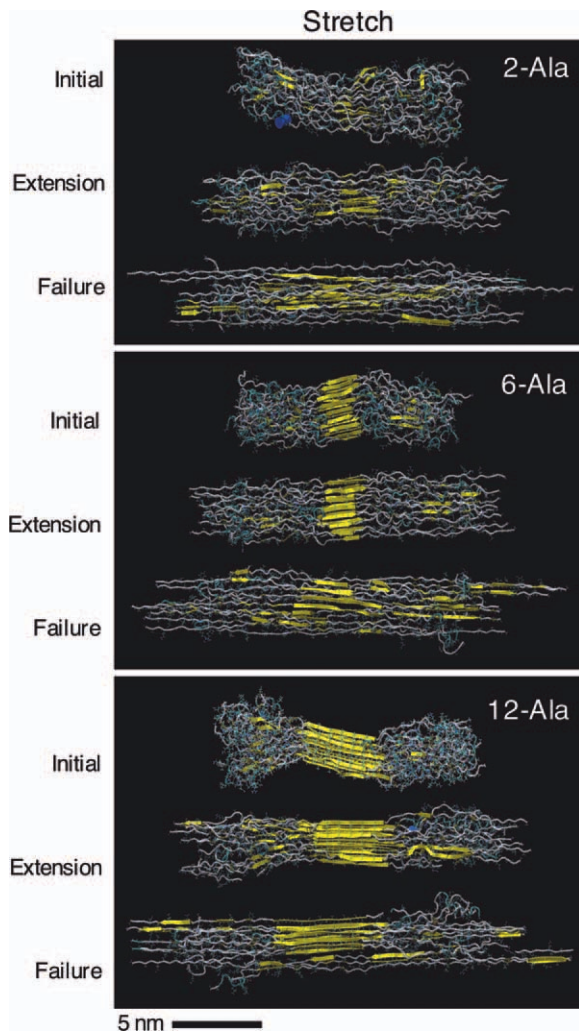


FIGURE 3 Snapshots during deformation for stretch test cases. For each case of poly-Ala length, the initial structure elongates as the semi-amorphous regions uncoil. Following this, the β -sheet crystal fails catastrophically in multi-lap shear.

The forces required to peel the β -sheet crystals are on the scale of hundreds of piconewtons (Figures 5d and 5e), one order of magnitude smaller than the forces required for shearing. The peel tests reveal that the forces required to peel apart the semi-amorphous strands surrounding each crystal (as in Figure 5a) are between 130% and 150% higher for all cases of poly-Ala length than the forces required to initialize direct cleavage of the crystal in the Y-configuration (as in Figure 5b). For both starting configurations, the peeling tests are stopped when the crystal has been completely cleaved (as in Figure 5c). Like the differences between stretch and pull-out cases, differences in the specific loading conditions of the peel tests show a large impact on the results even for the same case of poly-Ala length.

The cleavage-initializing force in the Y-configuration increases from the 2-Ala case to the 6-Ala case, then remains

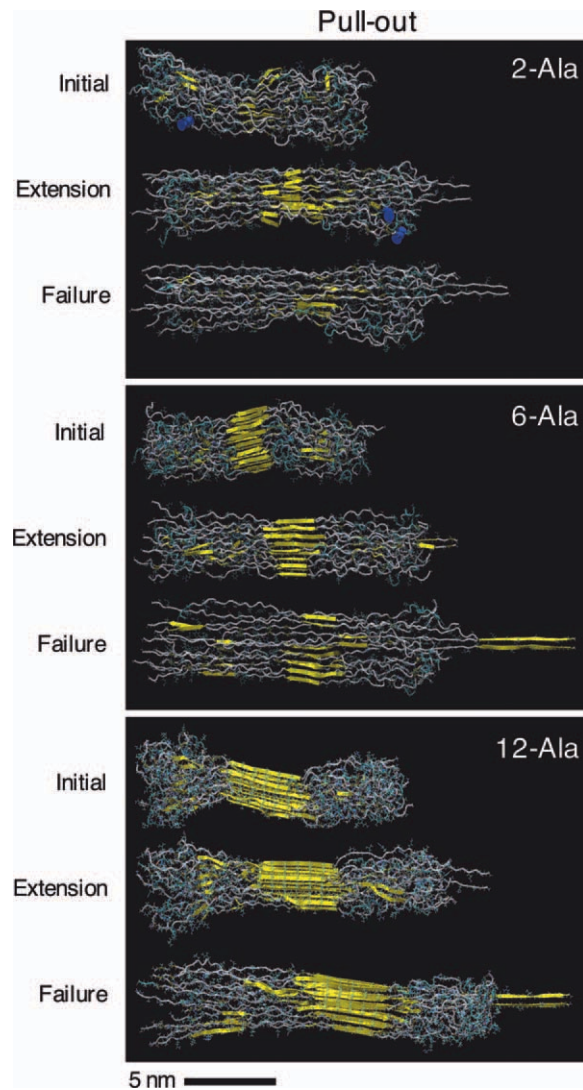


FIGURE 4 Snapshots during deformation for pull-out test cases. For each case of poly-Ala length, the initial structure elongates as the constrained semi-amorphous regions are pulled by the β -sheet crystal and uncoil, while the free semi-amorphous regions dissipate the force in pseudo-plasticity. Following this, the β -sheet crystal fails in double shear.

constant to the 12-Ala case. This result implies a saturation of the peeling resistance of a clearly defined β -sheet crystal above a critical length in the backbone direction, although correlations to the crystal size in the side-chain or H-bond directions are not yet clear. However, the saturation in peeling resistance is mitigated by the semi-amorphous regions, which provide protection from crystal cleavage that continues to increase with crystal length in the backbone direction.

Mitigation of peeling resistance saturation by the semi-amorphous regions suggests a similar protecting mechanism during multi-lap shearing of the crystal, i.e., stretch and pull-out conditions. Previous computational studies of

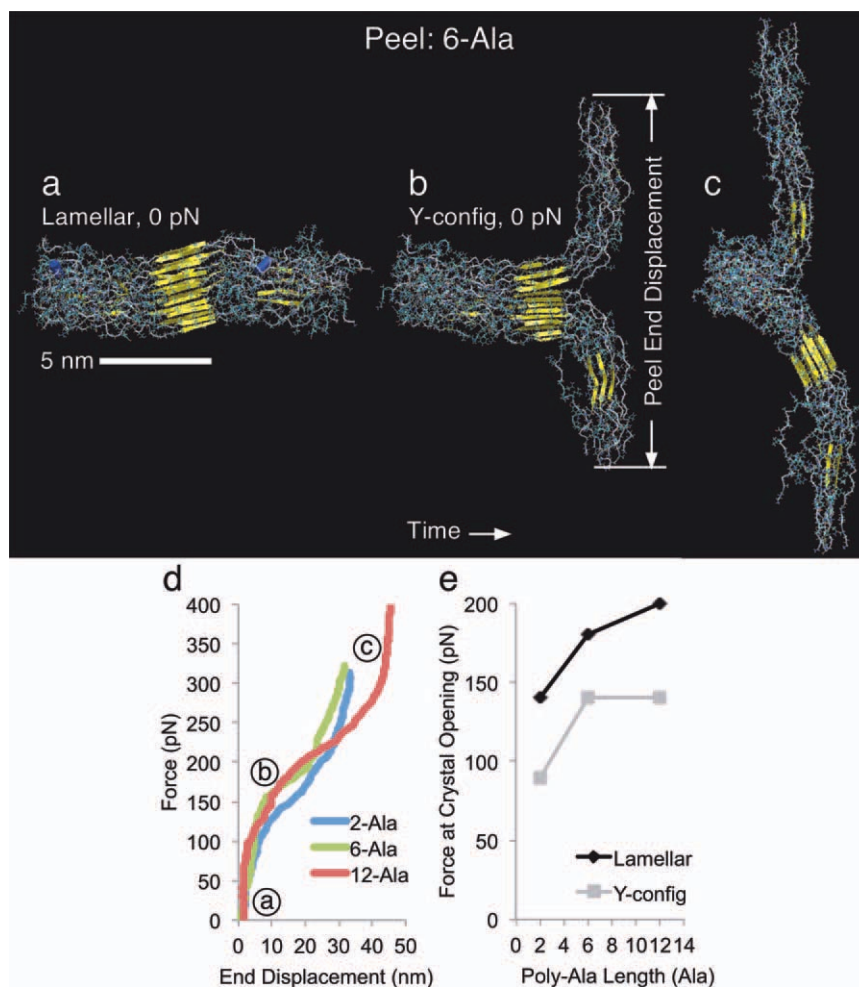


FIGURE 5 Snapshots and mechanical behavior for peel test cases. Two peeling cases are considered: (a) starting from the equilibrated structure and (b) starting with the crack tip at the edge of the β -sheet crystal. (c) Testing is complete when the protein has totally peeled. (d) The force vs. end displacement profiles for the lamellar case indicate softening when the crack ruptures the ordered H-bonds within the crystal, corresponding to the snapshot in (b). (e) The force at which the crystal peels illustrates the effects of different crystal lengths as well as initial geometries. During testing, the unloaded end of the protein does not displace. Water is hidden in this study for clarity, but remains surrounding the protein during testing.

isolated β -sheet crystals reveal a saturation in H-bond cooperativity at a critical length of 3–4 H-bonds,⁴⁵ beyond which each additional H-bond does not fully contribute to the overall shear strength. Such saturation is not observed in the above stretch and pull-out tests due to the pseudo-plasticity afforded by the semi-amorphous regions that diverts the direct loading on the crystal. Furthermore, when the central 2-Ala and 6-Ala β -sheet crystals are isolated and equilibrated alone, they prove unstable and quickly fall apart. The 12-Ala crystal remains largely intact, but loses β -stranded content at the edges. This suggests that the semi-amorphous regions pre-stress the crystals into a stable-stacked form and are therefore integral to the effective strength of the crystal.

Distribution of β -Sheet Content During Deformation

To reveal at what residues and forces these β -sheet transitions occur, i.e., the formation and growth of pseudo-plastic zones preceding failure, a colormap of local β -strand conformation is presented in Figure 6. The stretch and pull-out test results reveal that ultimate strength of the MaSp1 unit cell depends on more than just the initial crystals size. Because of the strain-hardening mechanism, i.e., the strain-induced transition from random coil conformation to β -sheet, a higher β -sheet content is present closer to failure than in the initial structure.

For all cases, the highest concentration of β -sheet is within the poly-Ala segment, shown as a gray box in Figure 6, yet

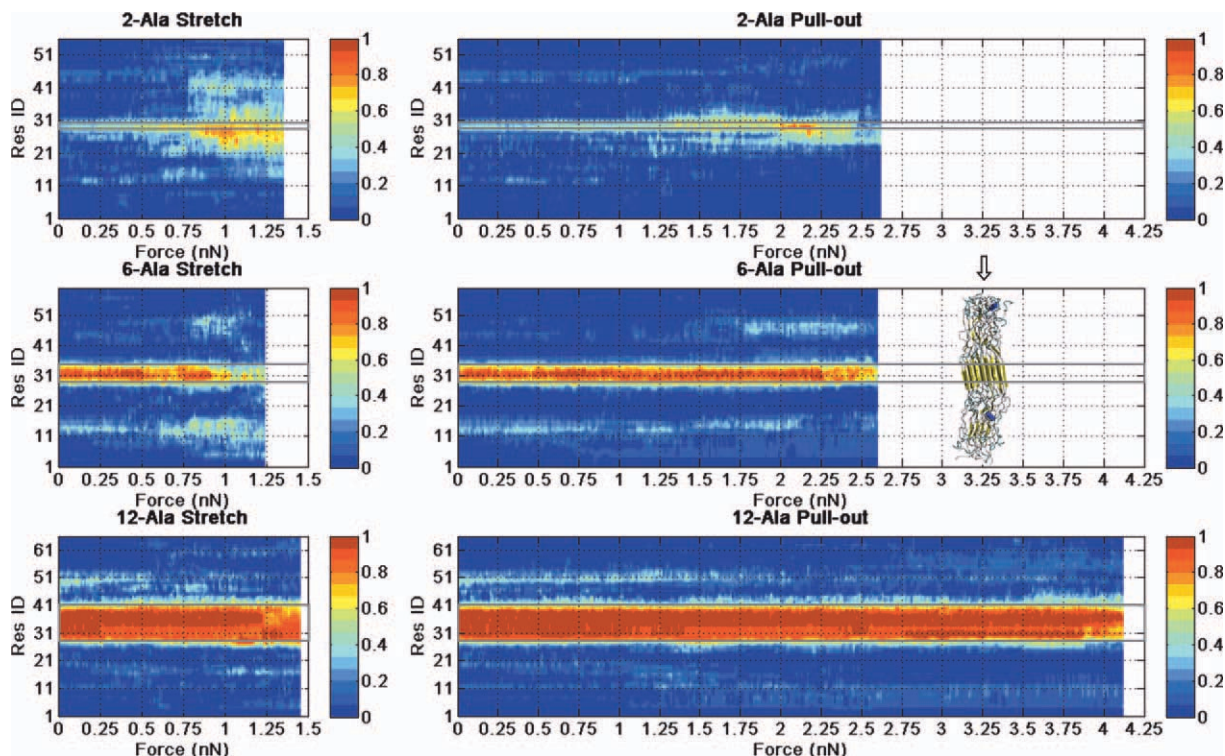


FIGURE 6 Colormaps showing β -sheet distribution during mechanical testing and illustrating the strain-induced growth of β -sheets as the semi-amorphous regions are elongated and aligned in parallel. Poly-Ala residues are outlined in a gray box for each case. The colormap value represents the percentage of strands exhibiting β -strand conformation at each residue, illustrated by the cartoon representation at the arrow.

almost totally absent in the semi-amorphous Gly-rich regions. Although some secondary crystal formation is observed, they are less pronounced than the central poly-Ala crystal. The pull-out tests show failure forces 2–2.7 times higher than for the stretch tests with the same initial structures and poly-Ala lengths but different loading conditions. For both tests, the failure force depends on the health of the central crystal, which is a subjective measure of the distribution of β -strand in and around the site of the initial crystal before loading. For stretch tests, the central crystal experiences direct loading at a lower force, while for pull-out tests, a pseudo-plastic zone, which includes the formation of small secondary crystals and dulling of the edges of the central crystal, is more evident and delays direct loading of the central crystal via β -sheet transitions in the semi-amorphous regions.

A visual representation of the health of the central crystal can be inferred from the amount of β -strand conformation within central crystal region as well as from the sharpness of the transition from high to low concentration. For the 2-Ala stretch case, the poly-Ala region transitions to a much higher concentration of β -sheet between 0.75 and 1.0 nN as formerly coiled strands are straightened and aligned, and a

large pseudo-plastic zone develops to surround the crystal. After 1.25 nN, the small crystal begins to shear directly, and the crystal deteriorates just before failure. The 6-Ala and 12-Ala cases show similar secondary crystal formation around 0.75–1.0 nN, but less of a pseudo-plastic zone develops around the central crystal. These bands of small secondary crystals form near the residue numbers corresponding to (GGLGSQ) of the sequence. Leucine (L) is hydrophobic, similar to Alanine, and may encourage the formation of these secondary crystals in a mechanism similar to the Leucine interactions of a Leucine Zipper. For the case of 2-Ala in this study, the organization of the initial crystal is very poor, and this may allow the semi-amorphous regions to be more globular than lamellar. On the other hand, the 6-Ala and 12-Ala cases show well-defined initial crystals that may organize the semi-amorphous regions and bring the Leucine into close proximity, especially as the semi-amorphous regions are straightened and aligned during loading, and thus allowing the formation of the secondary crystals. The reorganization of the semi-amorphous regions and formation of secondary crystals may be key to the superior toughness of 6-Ala and 12-Ala cases over 2-Ala. The β -sheet content and distribution

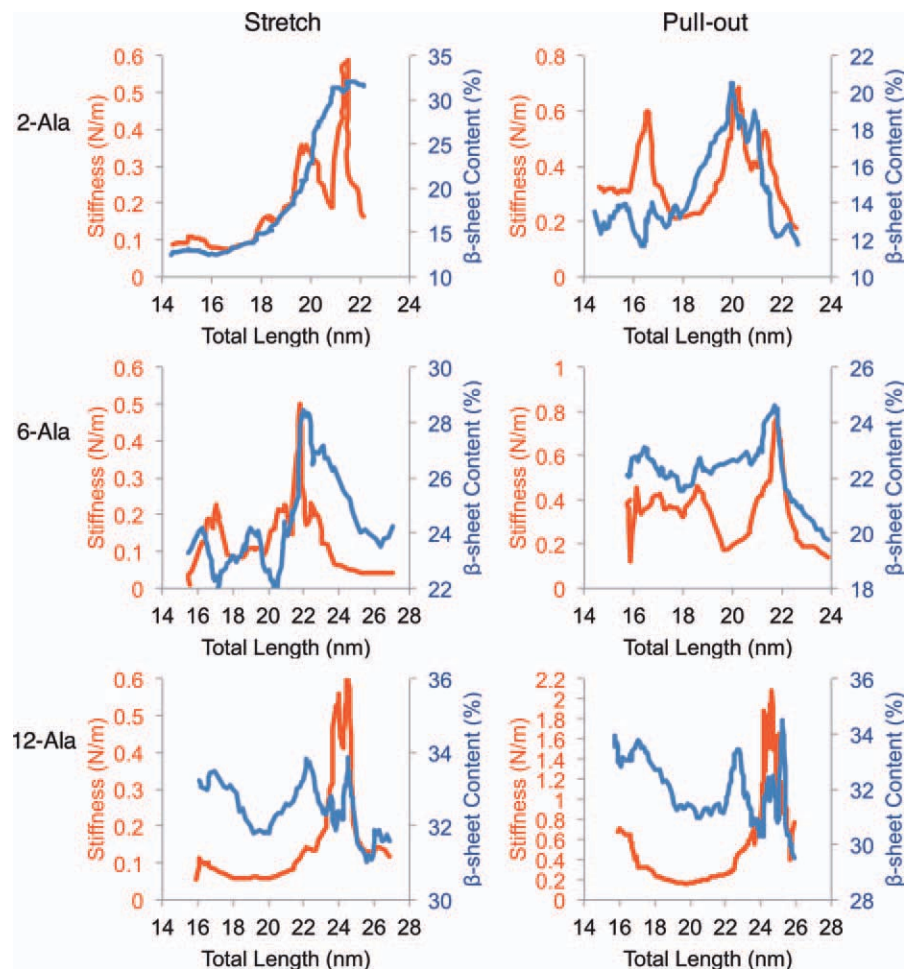


FIGURE 7 Total β -sheet content (blue) correlates closely to stiffness (red) for testing with explicit solvent. A characteristic drop in stiffness marks the beginning of a strain-hardening mechanism: a sudden increase in β -sheet content as strands are straightened and aligned. Preceding failure, β -sheet content decreases rapidly as H-bond clusters are ruptured in shear.

of the 6-Ala case is similar to the 2-Ala case preceding failure, and shows a similar failure force. Because of a negligible development of a pseudo-plastic zone, the central crystal of the 12-Ala case is similarly directly loaded and fails in shear at nearly the same force. Snapshots of the stretch tests of each test case, shown in Figure 3, illustrate the formation and growth of secondary crystals as strands are extended and aligned in parallel.

The pull-out tests results show similar trends, but at forces 2.0–2.7 times higher. For the 2-Ala stretch case, the poly-Ala region transitions to a much higher concentration of β -sheet now between 2.0 and 2.25 nN as formerly coiled strands are straightened and aligned, and a large pseudo-plastic zone develops to surround the crystal. After 2.25 nN, the small crystal begins to shear directly, but the pseudo-plastic zone carries the load to a much higher failure force than in the stretch test. This loading of the pseudo-plastic zone is the

softened third regime preceding failure that was observed in the force/length plots in Figures 2a and 2b. The 6-Ala pull-out case shows a similar development of a pseudo-plastic zone around 2.0 nN, yet deterioration of the central crystal appears more gradual with these loading conditions. The 12-Ala case also begins with a clearly defined central crystal, but slowly loses crystal definition at the edges, seen in Figure 6 as a sharp edge from red to blue becoming a wider gradient. Beyond 2.75 nN, the edges of the central crystal steadily decrease in definition, yet the work required to elongate and untangle the surrounding semi-amorphous regions extends the life of the crystal to above 4 nN.

Correlation of β -Sheet Content to Stiffness

The instantaneous β -sheet content correlates closely with stiffness for both tests, as shown in Figure 7. As cross-sectional

area and volume of the unit cell is difficult to define at the molecular scale in solvated conditions, stiffness is presented as a more convenient metric than engineering stress. Stiffness, in this study, is defined as the instantaneous slope of the force/length curves. While values may vary depending on simulation parameters, e.g., pulling rate, the authors hold the trends to be consistent. For small crystals, stiffness increases as β -sheet content increases. For large crystals, stiffness increases despite a negligible change in total β -sheet content, indicating the prevalence of another deformation mechanism such as the restructuring of the semi-amorphous strands and crystal edges. The results outlined in Figure 7 suggest that the wildtype 6-Ala case represents a transition between these two situations. This compromise may be advantageous for the behavior at larger length scales. For all cases, peaks in β -sheet content match peaks in stiffness. This is less evident in 12-Ala cases, however, because total β -sheet content ranges only within 3–4% of the initial value, as opposed to 2-Ala cases ranging 10–20% around the initial value. Differences in stiffness profiles brought by the differences in the loading conditions of the stretch and pull-out also become evident.

A characteristic valley in stiffness marks the beginning of the strain-hardening mechanism: a sudden increase in β -sheet content as strands are straightened and aligned. All cases also show a coinciding sudden decrease in β -sheet content and stiffness immediately preceding failure as H-bond clusters are ruptured in shear. There exists a transition in the ways crystal size and loading conditions affect the stiffness profiles. Small crystals such as those of the 2-Ala case are similar in their range in stiffness but not in the shapes of the stiffness profiles. In particular, the 2-Ala cases both range in stiffness from 0.1 to 0.7 N/m, but the pull-out case shows two stiff peaks and maintains a higher average stiffness throughout. However, the 2-Ala pull-out case reaches only 20% β -sheet content, 0.6 times the maximum β -sheet content of the 2-Ala stretch test (33%). In contrast, the 12-Ala cases show nearly identical stiffness profiles and ranges in β -sheet content, yet the ranges in stiffness are very different. The stretch case reaches only 0.6–0.7 N/m, close to the maximums of the 2-Ala and 6-Ala cases in stretch, while the 12-Ala case in pull-out reaches a stiffness near 2 N/m. The combination of the 12-Ala case crystal and central pull-out loading conditions results in a clearly superior unit cell using relatively soft, extensible semi-amorphous regions to mitigate direct damage to the β -sheet crystal and thereby overcome a predicted H-bond saturation length in similar β -sheet arrays. Though the edges of the 12-Ala central crystal steadily decrease in definition, the work required to elongate and untangle the surrounding semi-amorphous regions delays total failure of the crystal.

CONCLUSION

Nanomechanical testing revealed that the combination of the 12-alanine length case and central pull-out loading conditions results in delayed failure using a hierarchy of strong β -sheets and soft, extensible semi-amorphous regions to overcome a predicted H-bond saturation.⁴⁵ This work constitutes the most near-native study to-date of the nanomechanical behavior of dragline silk proteins. Building upon previous computational studies that used similar methods for structure prediction and mechanical analysis, i.e., REMD and force-control loading, this study presents the first mechanical tests of predicted β -sheet crystals in TIP3P explicit solvent, the first parametric study of the effects of modifying the wildtype poly-alanine segment length to values outside the range naturally observed for MaSp on structure prediction and nanomechanical behavior, and the first comparison between previously published loading conditions, i.e., the stretch test, and the novel pull-out loading conditions that are hypothesized to be more appropriate for modeling of the in situ loading of the cross-linking β -sheet crystal. While the initial total β -sheet contents and crystal sizes are very different for test cases with poly-Ala lengths of 2-, 6-, or 12-Ala, the unit cells' mechanical behaviors and forces at failure are very similar for the stretch test loading conditions, no matter the initial crystal size. The pull-out tests show similar strain-hardening but with failure forces 1.9–2.4 times higher than those of the stretch tests. The combination of the 12-Ala case crystal and central pull-out loading conditions result in a clearly superior unit cell using relatively soft, extensible semi-amorphous regions to mitigate direct damage to the β -sheet crystal and thereby overcome a predicted H-bond saturation length in similar β -sheet arrays. Though the edges of the 12-Ala central crystal steadily decrease in definition, the work required to elongate and untangle the surrounding semi-amorphous regions delays total failure of the crystal.

While the 12-Ala case in pull-out loading shows the highest shear strength and work-to-failure of the tested cases, such a high shear strength may be a disadvantage. The size and mechanical behavior of such large crystals may deter failure mechanisms of the fibrillar network at larger length scales, and this may in part explain the absence of such a long poly-alanine repeat unit in nature. Further atomistic studies are needed to define the effects of solvent (e.g., pH) and geometry (e.g., length of the semi-amorphous regions). Methods such as coarse-grain modeling are needed to investigate viscoelasticity and supercontraction at larger length scales of the fibrillar network and connectivity among crystals. In addition, the poly-Ala repeat unit is the most metabolically expensive peptide segment to synthesize,⁴⁶ and the resulting macroscopic web behavior may not provide the

advantages to warrant the additional energy cost. However, the 6-Ala (i.e., wildtype) case results in a clearly defined crystal that may be integral to other failure mechanisms of the fibrillar network that have yet to be simulated. In light of the differences observed for two similar but fundamentally different loading conditions explored in this study, future parametric studies in peptide sequence to optimize bulk fiber properties must involve variations in simulated nanomechanical loading conditions to properly assess the effects of the changes in peptide sequence. Understanding the behavior of the crystal node at the molecular scale and its impact on the larger fibrillar network is critical for potentially bypassing strength and vastly improving silk for medical and textile purposes as well as synthetic elastomers and polymer or aramid fiber composites with a similar molecular structure and noncovalent bonding for aerospace, armor, and medical applications.

REFERENCES

- Vollrath, F.; Knight, D. P. *Nature* 2001, 410, 541–548.
- Termonia, Y. *Macromolecules* 1994, 27, 7378–7381.
- Simmons, A. H.; Michal, C. A.; Jelinski, L. W. *Science* 1996, 271, 84–87.
- Shao, Z. Z.; Vollrath, F. *Nature* 2002, 418, 741.
- Becker, N.; Oroudjev, E.; Mutz, S.; Cleveland, J. P.; Hansma, P. K.; Hayashi, C. Y.; Makarov, D. E.; Hansma, H. G. *Nat Mater* 2003, 2, 278–283.
- Hayashi, C. Y.; Shipley, N. H.; Lewis, R. V. *Int J Biol Macromol* 1999, 24, 271–275.
- Gosline, J.; Guerette, P.; Ortlepp, C.; Savage, K. *J Exp Biol* 1999, 202, 3295–3303.
- Gatesy, J.; Hayashi, C.; Motriuk, D.; Woods, J.; Lewis, R. *Science* 2001, 291, 2603–2605.
- Brooks, A. E.; Steinkraus, H. B.; Nelson, S. R.; Lewis, R. V. *Biomacromolecules* 2005, 6, 3095–3099.
- Hayashi, C. Y.; Lewis, R. V. *J Mol Biol* 1998, 275, 773–784.
- Holland, G. P.; Creager, M. S.; Jenkins, J. E.; Lewis, R. V.; Yarger, J. L. *J Am Chem Soc* 2008, 130, 9871–9877.
- Hinman, M. B.; Lewis, R. V. *J Biol Chem* 1992, 267, 19320–19324.
- Guerette, P. A.; Ginzinger, D. G.; Weber, B. H. F.; Gosline, J. M. *Science* 1996, 272, 112–115.
- Sponner, A.; Schlott, B.; Vollrath, F.; Unger, E.; Grosse, F.; Weisshart, K. *Biochemistry* 2005, 44, 4727–4736.
- Thiel, B. L.; Guess, K. B.; Viney, C. *Biopolymers* 1997, 41, 703–719.
- van Beek, J. D.; Hess, S.; Vollrath, F.; Meier, B. H. *Proc Natl Acad Sci USA* 2002, 99, 10266–10271.
- Lefevre, T.; Rousseau, M. E.; Pezolet, M. *Biophys J* 2007, 92, 2885–2895.
- Keten, S.; Buehler, M. J. *Appl Phys Lett* 2010, 96, 153701–152703.
- Keten, S.; Xu, Z.; Ihle, B.; Buehler, M. J. *Nat Mater* 2010, 9, 359–367.
- Dicko, C.; Vollrath, F.; Kenney, J. M. *Biomacromolecules* 2004, 5, 704–710.
- Rammensee, S.; Slotta, U.; Scheibel, T.; Bausch, A. R. *Proc Natl Acad Sci USA* 2008, 105, 6590–6595.
- Du, N.; Liu, X. Y.; Narayanan, J.; Li, L.; Lim, M. L. M.; Li, D. *Biophys J* 2006, 91, 4528–4535.
- Wu, X.; Liu, X.-Y.; Du, N.; Xu, G.; Li, B. *Appl Phys Lett* 2009, 95, 093703.
- Philip, M. C.; Stephen, A. F.; Margaret, A. A.; John, W. S.; David, L. K.; Adams, W. W.; Ronald, K. E.; David, M.; Deborah, L. V. *Polym Adv Technol* 1994, 5, 401–410.
- Porter, D.; Vollrath, F.; Shao, Z. *Eur Phys J E* 2005, 16, 199–206.
- Riekel, C.; Vollrath, F. *Int J Biol Macromol* 2001, 29, 203–210.
- Trancik, J. E.; Czernuszka, J. T.; Bell, F. I.; Viney, C. *Polymer* 2006, 47, 5633–5642.
- van Beek, J. D.; Kummerlen, J.; Vollrath, F.; Meier, B. H. *Int J Biol Macromol* 1999, 24, 173–178.
- Jenkins, J. E.; Creager, M. S.; Lewis, R. V.; Holland, G. P.; Yarger, J. L. *Biomacromolecules* 2010, 11, 192–200.
- Rousseau, M. E.; Lefevre, T.; Beaulieu, L.; Asakura, T.; Pezolet, M. *Biomacromolecules* 2004, 5, 2247–2257.
- Rousseau, M. E.; Lefevre, T.; Pezolet, M. *Biomacromolecules* 2009, 10, 2945–2953.
- Porter, D.; Vollrath, F. *Soft Matter* 2008, 4, 328–336.
- Brooks, C. L. *Curr Opin Struct Biol* 1995, 5, 211–215.
- Ma, B. Y.; Nussinov, R. *Curr Opin Chem Biol* 2006, 10, 445–452.
- Buehler, M. J.; Keten, S.; Ackbarow, T. *Prog Mater Sci* 2008, 53, 1101–1241.
- Kummerlen, J.; vanBeek, J. D.; Vollrath, F.; Meier, B. H. *Macromolecules* 1996, 29, 2920–2928.
- Bratzel, G. H.; Buehler, M. J. *J Mech Behav Biomed Mater* (in review) 2011. Doi: 10.1016/j.jmbbm.2011.07.012.
- Kinahan, M. E.; Filippidi, E.; Koster, S.; Hu, X.; Evans, H. M.; Pfohl, T.; Kaplan, D. L.; Wong, J. *Biomacromolecules* 2011, 12, 1504–1511.
- Nova, A.; Keten, S.; Pugno, N.; Redaelli, A.; Buehler, M. J. *Nano Letters* 2010, 10, 2626–2634.
- Darden, T. *J Chem Phys* 1993, 98, 10089.
- Keten, S.; Buehler, M. J. *J R Soc Interface* 2010, 7, 1709–1721.
- Humphrey, W.; Dalke, A.; Schulten, K. *J Mol Graphics* 1996, 14, 33–38.
- Frishman, D.; Argos, P. *Protein Struct Funct Bioinformatics* 1995, 23, 566–579.
- Qin, Z.; Buehler, M. *J Phys Rev Lett* 2010, 104, 198304.
- Keten, S.; Buehler, M. *J Nano Lett* 2008, 8, 743–748.
- Craig, C. L.; Hsu, M.; Kaplan, D.; Pierce, N. E. *Int J Biol Macromol* 1999, 24, 109–118.

Reviewing Editor: David Nate Breslauer